Electronic Supplementary Material (ESI) for Journal of Materials Chemistry A.
This journal is © The Royal Society of Chemistry 2020

Supporting Information

High-Performance Filters from Biomimetic Wet-Adhesive Nanoarchitectured Networks

Hui Liu,[a] Shichao Zhang,[b] Lifang Liu,[a] Jianyong Yu,[b] and Bin Ding*[ab]

[a] State Key Laboratory for Modification of Chemical Fibers and Polymer Materials, College of Textiles, Donghua University, Shanghai 201620, China.

[b] Innovation Center for Textile Science and Technology, Donghua University, Shanghai 200051, China.

Supporting Information contains:

Supplementary Methods

Air filtration performance measurement

The filtration efficiency and pressure drop of the biomimetic nanofiber-net filters were measured using a TSI Model 8130 automated filter tester (TSI Inc.). 2 wt% NaCl aqueous solution was used to process the monodisperse aerosols with a mass median diameter of 0.3 μm and a geometric standard deviation of <1.86. The neutralized NaCl aerosols could be fed into a filter holder and pass through the filter with an effective area of 100 cm^2 on the demand air flow. The removal efficiencies of the filters were measured by detecting the aerosol concentrations in the upstream and downstream of the particle airflow.

Long-term recycling $PM_{2.5}$ purification measurement

The $PM_{2.5}$ recycling clear measurement was performed in a 0.1 m^3 enclosed cabin using the nanofiber-net filter with >99% removal efficiency. The model particles were generated by burning cigarettes which have similar ingredients to the real $PM_{2.5}$ pollution, and most particle diameters were in the range of <1 μm. Then, severely polluted air environment ($PM_{2.5}$ concentration >500 μg m^{-3}) was controlled artificially. And a nanofiber-net filter with area of ~25 cm^2 was used to purify the polluted air to a good level of 35 μg m^{-3} under a continuous airflow of 14 L min^{-1} generated by an axial fan. The value of $PM_{2.5}$ concentrations was tested using a detection instrument (SDL 301, Nova Fitness). We recorded the data of $PM_{2.5}$ concentrations once at most per minute until 35 μg m^{-3}. The recycling performance was evaluated by testing for 10 cycles.

Cycling separation performance measurement

To exam the reusability of the biomimetic nanofiber-net filters, a cycling separation for TiO_2 suspension was performed using a dead-end filtration device. Disc membranes with effective area

of 2 cm^{-2} were fixed in the test system and prewetted by pure water. Then the 100 ppm TiO_2 nanoparticle (diameter 200–400 nm) suspension were kept pouring onto the membranes under external driving pressures of 5 kPa. We recorded the initial and final rejection efficiencies and permeation fluxes of each cycle (10 min) and then backwashed the membrane with clean water 2 times before the next cycling test. The testing was lasted for 50 min.

Dye adsorption performance measurement

For the dye adsorption experiments, an aqueous solution of MB with initial concentration of 20 mg L^{-1} was chosen as the model contaminant. Then about 10 mg PAN/PDA nanofiber-net membranes was added into 50 mL MB solution under a magnetic stirring of 150 rpm at room temperature. At different time intervals, a certain amount of the supernatant solutions were withdrawn and measured by UV spectrophotometer at the wavelength of 632 nm.

Supplementary Figures

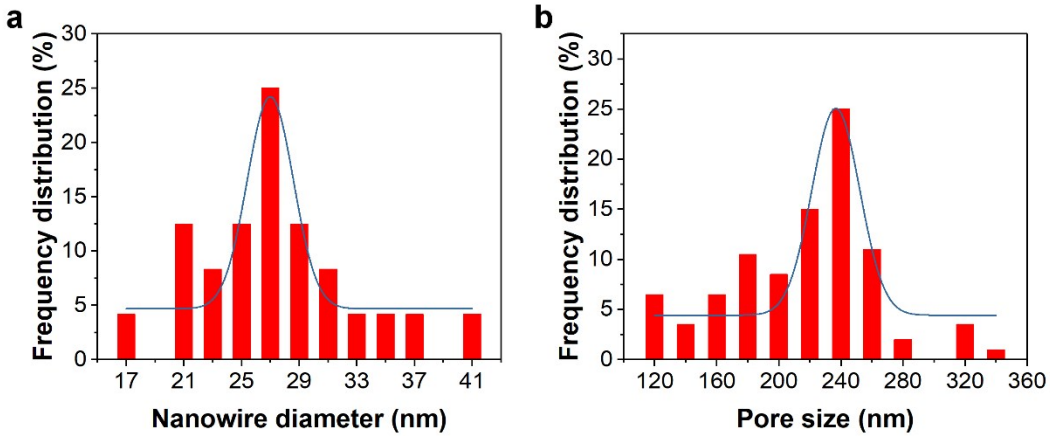

Figure S1. (a) Nanowire diameter and (b) pore size distribution of the 2D nanonets in PAN/PDA nanofiber-nets.

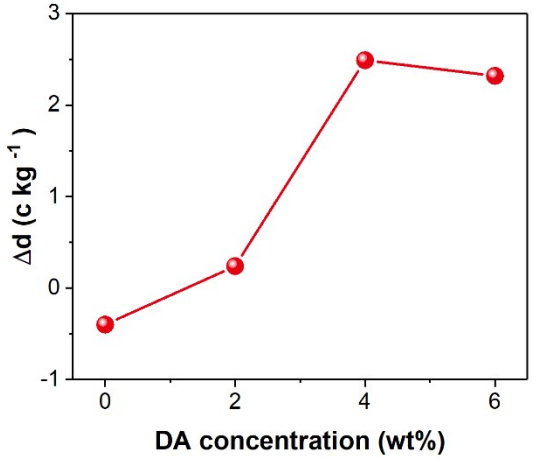

Figure S2. Differences between the droplet thresholds and the tested charge densities of the fluid with various DA concentrations.

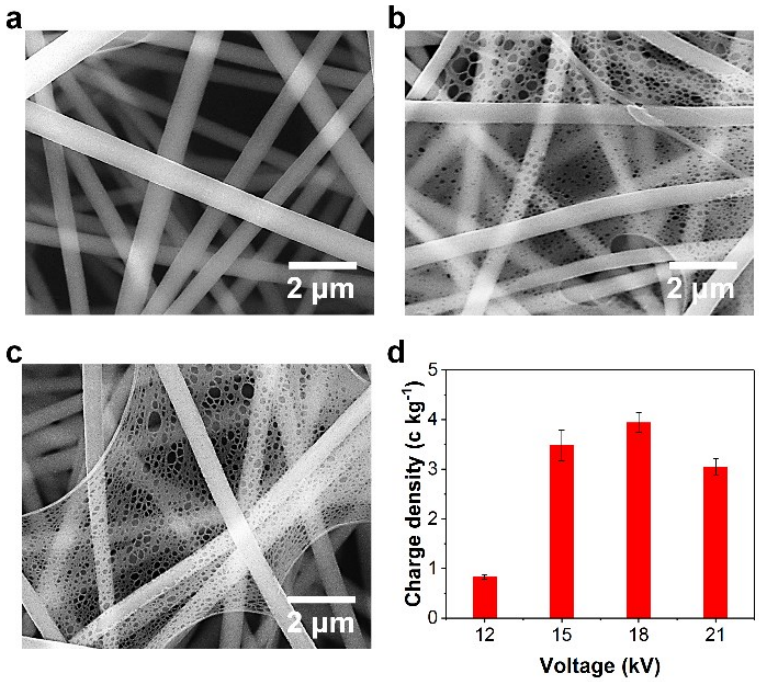

Figure S3. SEM images of the nanofiber membranes obtained under different voltages of (a) 12, (b) 18, and (c) 21 kV. (d) Charge densities of the fluids during electrospinning/netting process under different voltages.

Obviously, only nanofibers generated under the voltage of 12 kV due to the low charge density of the liquid of 0.83 c kg^{-1} (Fig. S3d) that was less than the droplet threshold (0.99 c kg^{-1}). Abundant nanofiber-nets with partly non-porous structures created when the voltage increased to 18 kV, which was ascribed to the high droplet formation probability and inadequate phase separation. Further increasing the voltage to 21 kV, the coverage of the nanonets slightly decreased because of their reduced charge density (3.05 c kg^{-1}) probably resulted from the increased fiber formation mass per unit time at the higher voltage.

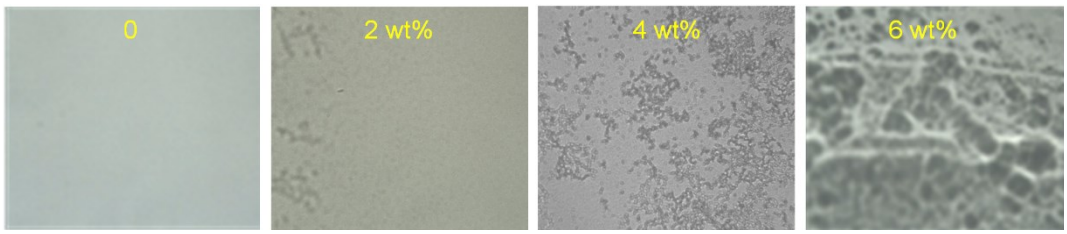

Figure S4. Optical images of PAN solutions with different DA concentrations for 10 min evaporation.

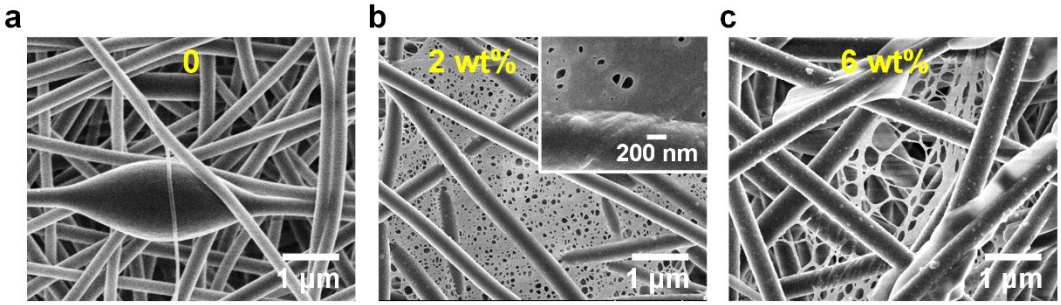

Figure S5. SEM images of a) beaded nanofibers, b) nanofiber/films, c) defective nanofiber/nets obtained from PAN solutions with different DA concentrations after polymerization.

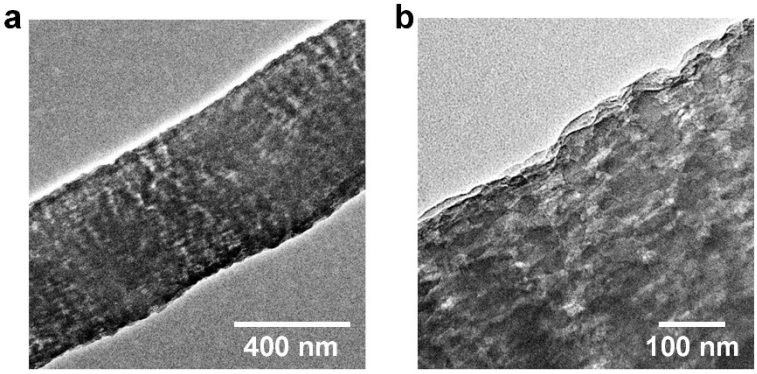

Figure S6. TEM images of the PAN/PDA nanofibers. The PDA coating layer was uniformly distributed on the surface of the nanofibers and formed some small protuberances.

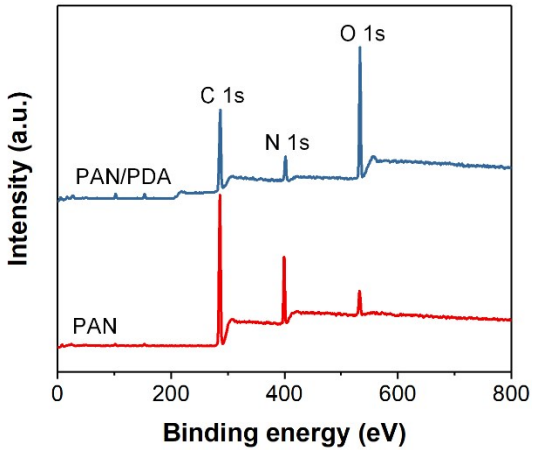

Figure S7. XPS spectra of the PAN nanofibers and the PAN/PDA nanofiber-nets.

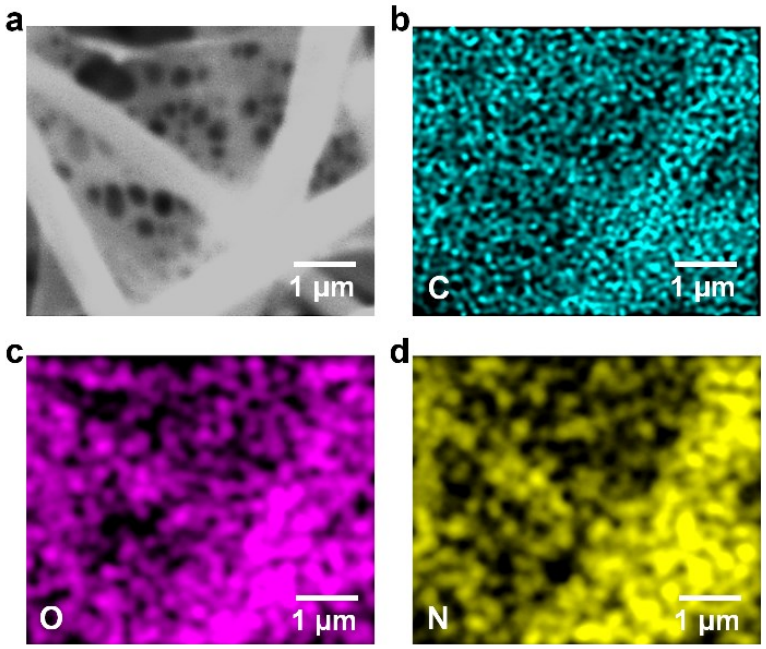

Figure S8. (a) SEM image of PAN/PDA nanofiber-nets, and their corresponding elemental mapping images of (b) C, (c) O, and (d) N. Obviously, O element was uniformly distributed on surface of the fibers and the networks, confirming the PDA component was also evenly distributed on the nanowire surface in 2D nanonets.

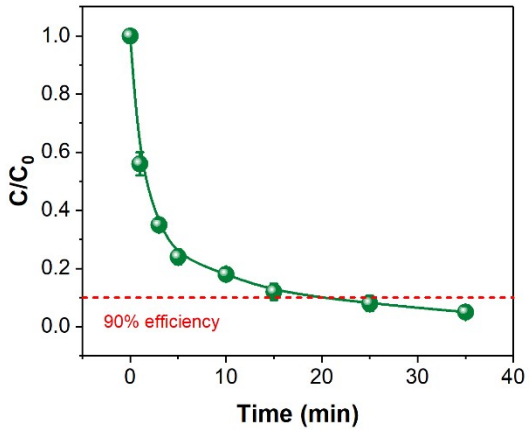

Figure S9. Dye adsorption performance of the nanofiber-nets.

A methylene blue (MB) static immersion adsorption process revealed that >98% of MB (20 mg L^{-1}, 50 mL) in the solution can be adsorbed by a small piece of nanofiber-nets within 35 min (Fig. S9). Such highly effective adsorption was ascribed to the enlarged surface area of the nanonets and the hydrogen bonding and electrostatic interaction between the negatively charged oxygen

functional groups of PDA and the amine groups in MB. In addition, we believe the PDA nanofiber-net membranes can also adsorb anionic dye in acidic solution but is not as efficient as the adsorption to cationic dyes.

Supplementary Tables

Table S1. Effect of DA concentration on the charge density of ejected fluids.

	TBAC concentration (wt%)	0	1	2	4
Theoretical calculation	ε (F m^{-1})	36.76*8.85*10^{-12}			
	ρ (kg m^{-3})	976			
	η (cps)	1326	1895	2232	2687
	γ (mN m^{-1})	21.52	23.15	22.35	22.64
	K (μS cm^{-1})	183	965	1632	2487
	D (m)	1.457*10^{-5}	1.307*10^{-5}	1.308*10^{-5}	1.314*10^{-5}
	$D_c = \sqrt{\frac{288\varepsilon\gamma}{\rho^2 D^3}}$ (c kg^{-1})	0.390	0.476	0.467	0.467
	$J_c = \sqrt{\frac{64\varepsilon\gamma}{\rho^2 D^3}}$ (c kg^{-1})	0.827	1.010	0.991	0.990
Experimental charge density	e/m (c kg^{-1})	0.43	1.25	3.48	3.31

Table S2. Contact angle (CA), overall surface energy (σ_S), polar component (σ_S^P) and non-polar component (σ_S^D) of PAN nanofiber, PAN nanofiber-nets and PAN/PDA nanofiber-nets.

Surface	CA (H_2O)	CA (CH_2I_2)	σ_S (mN m^{-1})	σ_S^P (mN m^{-1})	σ_S^D (mN m^{-1})
PAN nanofiber	65.3	53.2	43.22	10.75	32.47
PAN nanofiber-nets	42.8	30.5	62.16	18.15	44.01
PAN/PDA nanofiber-nets	8.5	25.6	76.37	30.43	45.94

Table S3. *Knudsen* numbers and flow regimes dependent on different ranges of fiber diameter under normal condition.

Fiber diameter (d)	Knudsen number ($Kn=2\lambda/d$)	Flow regimes
d > 132 μm	Kn < 0.001	Continuum flow
528 nm < d < 132 μm	0.001 < Kn < 0.25	Slip flow
13.2 nm < d < 528 nm	0.25 < Kn < 10	Transition flow
d < 13.2 nm	Kn > 10	Free molecular flow

Table S4. Filtration performance of some metallic microfiltration filters.

Type	**Mean pore size (μm)**	**Test particle size (μm)**	**Water flux (L m^{-2} h^{-1} bar^{-1})**	**Rejection efficiency (%)**	**Ref.**
Ni sheet	0.39	2 – 20	10000	100	1
Ni screen	2.5	3	10667	100	2
Commercially metal filters	5	2	23000	56	3
	1	2	8467	59	3

Generally, the pore size of the metallic microfiltration filters are usually large and their water flux are quite high, which is widely used for rapid filtration and coagulation pre-treatment (such as sediment/rust removal) in drinking water production. While for smaller particles or

microorganisms removal (for instance, bacteria with typical sizes of ~0.5–2 μm) in some high-precision filtration applications, such as medical application, the nanofiber-net filters with small pores might be more suitable and promising.

Supplementary Discussion

Ejection models of the charged fluids on Taylor cone apex

In this work, we first assume the diameter (*D*) of the Taylor cone apex obtained at the maximum curvature as the diameter of the ejected fluid (jet and droplet), which can be calculated by the following parametric equation:

$$D = \frac{1.4639 Q^{0.44} \varepsilon^{0.12} \eta^{0.32}}{K^{0.12} \gamma^{0.32}} \quad \text{(S1)}$$

Where Q is the volumetric flow rate of the fluid, ε is the ambient permittivity, η is the viscosity of the fluid, K is the conductivity of the fluid and γ is the surface tension of the fluid. Then systematically analyzing the forces acting on the charged Taylor cone apex found that, the gravity of the liquid could be negligible due to its tiny weight; thus the ejection modes (jet and droplet mode) are mainly driven by the competition between the Coulomb repulsion F_e and the hydrostatic pressure F_γ. And the basic prerequisite for both ejection modes is

$$F_e > F_\gamma \quad \text{(S2)}$$

For the jet mode, we assumed the fluid ejected from Taylor cone as a cylinder; thus, the hydrostatic pressure F_γ acted on the fluid is:

$$F_\gamma = \frac{\gamma}{R} \quad \text{(S3)}$$

and, the Coulomb repulsion F_e is expressed as:

$$F_e = \frac{e^2}{8\varepsilon\pi^2 R^2 l^2} \quad \text{(S4)}$$

In addition, the mass of the studied cylindrical fluid *m* is:

$$m = \frac{1}{4}\rho\pi D^2 l \tag{S5}$$

For the droplet mode, the fluid ejected from the Taylor cone was assumed to a sphere; thus the hydrostatic pressure F_γ caused by the surface tension is:

$$F_\gamma = \frac{2\gamma}{R} \tag{S6}$$

the Coulomb repulsion F_e is:

$$F_e = \frac{e^2}{32\varepsilon\pi^2 R^4} \tag{S7}$$

And the mass of the charged droplet *m* is:

$$m = \frac{1}{6}\rho\pi D^3 \tag{S8}$$

Where R is the radius of charged fluid, e is the charge carried on the fluid, ρ is the density of the fluid and l is the length of hypothetical cylindrical jet.

Therefore, the jet and droplet thresholds can be deduced based on solving the simultaneous equations, and the results are as follows:

$$\text{Jet mode: } J_c = \sqrt{\frac{64\varepsilon\gamma}{\rho^2 D^3}} \tag{S9}$$

$$\text{Droplet mode: } D_c = \sqrt{\frac{288\varepsilon\gamma}{\rho^2 D^3}} \tag{S10}$$

Obviously, the droplet threshold is affected by both the surface tension and the solution viscosity. And, both the solution surface tension and viscosity usually decrease with the increase of the temperature. Therefore, the droplet threshold would change with the variation of the temperature. However, it is difficult to say whether the threshold would increase or decrease

definitely, because the surface tension is in the numerator while the viscosity is in the denominator in the formula. In addition, despite controlling the network structure by tuning the temperature is feasible in theory; some limitations still remain in actual operation, such as the high or low solution temperature retention. Therefore, in this work, we choose the more facile and effective approach by introducing additives in the solution to tailoring the formation of nanonet structures.

Supplementary References

[1] W. Liu, and N. L. Canfield, J. Membr. Sci., 2012, **409**, 113-126.

[2] M. E. Warkiani, C. Lou, H. Liu, and H. Gong, Biomed. Microdevices, 2012, **14**, 669-677.

[3] R. Kim, S. Lee, and J. Kim, Desalination, 2005, **177**, 121-132.